

**Electronic Supplementary Material (ESI) for CrystEngComm.**

**This journal is © The Royal Society of Chemistry 2020**

## **Method to reduce the oil pressure during HPHT diamond synthesis: FEM simulations and experiments**

**Chunxiao Wang,<sup>a</sup> Hong-an Ma,<sup>\*a</sup> Liangchao Chen,<sup>\*b</sup> Xinyuan Miao,<sup>c</sup> Liang Zhao,<sup>d</sup> Xiaopeng Jia<sup>\*a</sup>**

<sup>\*a</sup>State Key Lab of Superhard Materials, Jilin University, Changchun 130012, China.

<sup>\*b</sup>School of Physics and Microelectronics, Zhengzhou University, Zhengzhou 450052, China.

### **Electronic Supplementary Information (ESI)**

**Electronic Supplementary Information (ESI) Available:** Simulation details, experimental methods, material parameters and experimental data.

#### **Table of Contents**

Finite element model and nonlinear algorithm .....	S2
1. Finite element analysis program ABAQUS.....	S2
2. Explicit nonlinear dynamic analysis algorithms .....	S3
3. Selection of unit type .....	S5
4. Selection of unit size .....	S7
5. Elastic-plastic constitutive relation model .....	S8
5.1 Elastic plasticity of materials .....	S8
5.2 Mises plasticity model .....	S9
5.3 Drucker-Prager (DP) plasticity model .....	S10
6. Finite element model .....	S11
7. Principle of mass support.....	S14
8. Boundary conditions .....	S15
9. Material parameters .....	S16
10. Experiment date: .....	S18
Notes and references .....	S19

---

## **Finite element model and nonlinear algorithm**

This paper used Solidworks CAD three-dimensional modeling software to establish a three-dimensional solid model of the SPD-6×1200 cubic anvil and high-temperature and high-pressure synthetic assembly cell. We imported it into the finite element analysis software ABAQUS to establish the finite element model of the quadratic tetrahedral element (C3D10M) mesh. The properties of the material were analyzed, and the constitutive relationship of the material was established. The establishment of the finite element model and simulation method laid the foundation for the finite element simulation of the pressure field in the cavity of the new pressurized block.

### **1. Finite element analysis program ABAQUS**

As a powerful finite element analysis software, ABAQUS can solve simple models, as well as some complex and large models. Due to its powerful solver module, when solving some highly nonlinear problems in actual engineering, it has unique advantages and is recognized as one of the most advanced software packages for nonlinear analysis in the industry. ABAQUS can solve a wide range of linear and nonlinear problems, as well as some complex coupled analyses, including thermal-mechanical coupled analysis, thermal-electric coupled analysis, fluid-structure coupled analysis, and mass diffusion analysis. It is widely used in scientific research fields such as aerospace, electronic appliances, automobile transportation, national defense, medical, petroleum and petrochemical, energy and power, material processing. Fig. S1 shows the application areas of ABAQUS software.

<b>Aerospace</b>	<b>Electronic</b>	<b>Medical treatment</b>	<b>Durable goods</b>
Lockheed Martin - JSF Boeing - 777 Airbus - Manufacturing	Motorola - Drop Tests Fujitsu - Computers Intel - Chip Integrity	Baxter - Equipment J&J - Stents Medtronic - Pacemaker	P&G — Packaging Kao - Hygiene Xerox - Copiers
<b>Car</b>	<b>Heavy industry</b>	<b>National defense</b>	<b>Material processing</b>
GM - Powertrain Honda - Transmission BMW - Durability	Paccar-Trucks Caterpillar - Machinery RR - Aero Engines	NNS - Aircraft Carriers Los Alamos - Stockpile Qinetiq - Submarines	Corus - Roll-Pass Dupont - Composites Kobe Steel - Metals
<b>Tires</b>	<b>Petroleum and Petrochemical</b>	<b>Energy power</b>	<b>Education</b>
Sumitomo - Auto Cooper - Auto Goodyear - Aircraft	ExxonMobil - Connectors Shell - Reservoirs Technip - Coflex - Risers	Alstom - Turbines British Energy - Nuclea IHI - Turbines	MIT - MEMS Cambridge - R&D IIT - Teaching

**Fig. S1** Application areas of ABAQUS software

## 2. Explicit nonlinear dynamic analysis algorithms

The explicit solution method and the implicit solution method are the two solution methods using finite element simulations. The explicit solution method can better solve highly nonlinear problems. ABAQUS/Explicit uses the central difference method to solve equations of motion, and the previous incremental step is used to solve the dynamic equation as a condition for the next step. The formula solves the dynamic balance equation, where  $M$  is the mass of the node, the acceleration is  $\ddot{u}$ , the external force is  $P$ , and the internal force is  $I$ . The product of nodal mass and acceleration is equal to the joint force.

$$M\ddot{u} = P - I$$

---

Since the explicit method for solving the acceleration of each incremental step of the step nodes together, the solution process is not complicated, which decreases calculation costs. Since the calculation results of each incremental step of the explicit analysis only depend on the calculation results of the previous step, the accuracy of this method is very high. During large-scale nonlinear analysis, because there are few incremental steps, the required calculation results can be completed quickly.

The following is a process of explicit dynamic analysis:

Node computing

(1) Dynamic equilibrium equation

$$\mathbf{M}\ddot{\mathbf{u}}|_{(t)} = (\mathbf{M})^{-1}(\mathbf{P} - \mathbf{I})|_{(t)}$$

(2) Both sides of the equation integrate time

$$\dot{\mathbf{u}}|_{t+\Delta t} = \dot{\mathbf{u}}|_t + \Delta t \left. \ddot{\mathbf{u}} \right|_{t+\frac{\Delta t}{2}}$$

Set when  $t$  is  $\Delta t$ , return to step (1)

Explicit analysis is particularly suitable for solving large-scale nonlinear dynamic problems. In explicit analysis, some discontinuous problems can be easily solved without iteration or convergence criteria, allowing high-precision results analysis to be performed quickly. Fig. S2 is a schematic diagram of the operation used to establish the explicit dynamic analysis step.

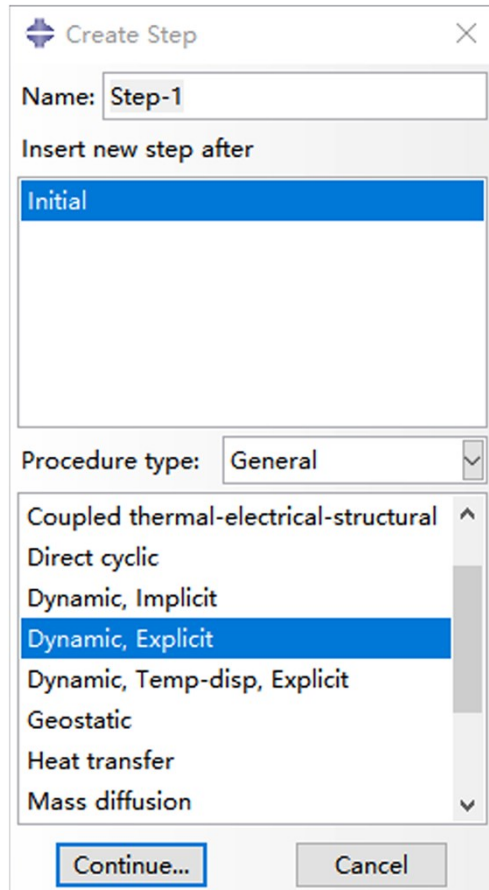


**Fig. S2** Explicit nonlinear dynamic analysis step operation diagram.

### **3. Selection of unit type**

ABAQUS has a very rich element library. It is necessary to select the appropriate element type according to the situation of the model and the analysis type. For different analysis types, the corresponding elements must be selected to generate a grid. The prerequisite for selecting the unit type is to improve the calculation accuracy and efficiency. Fig. S3 shows the most commonly used elements in ABAQUS.

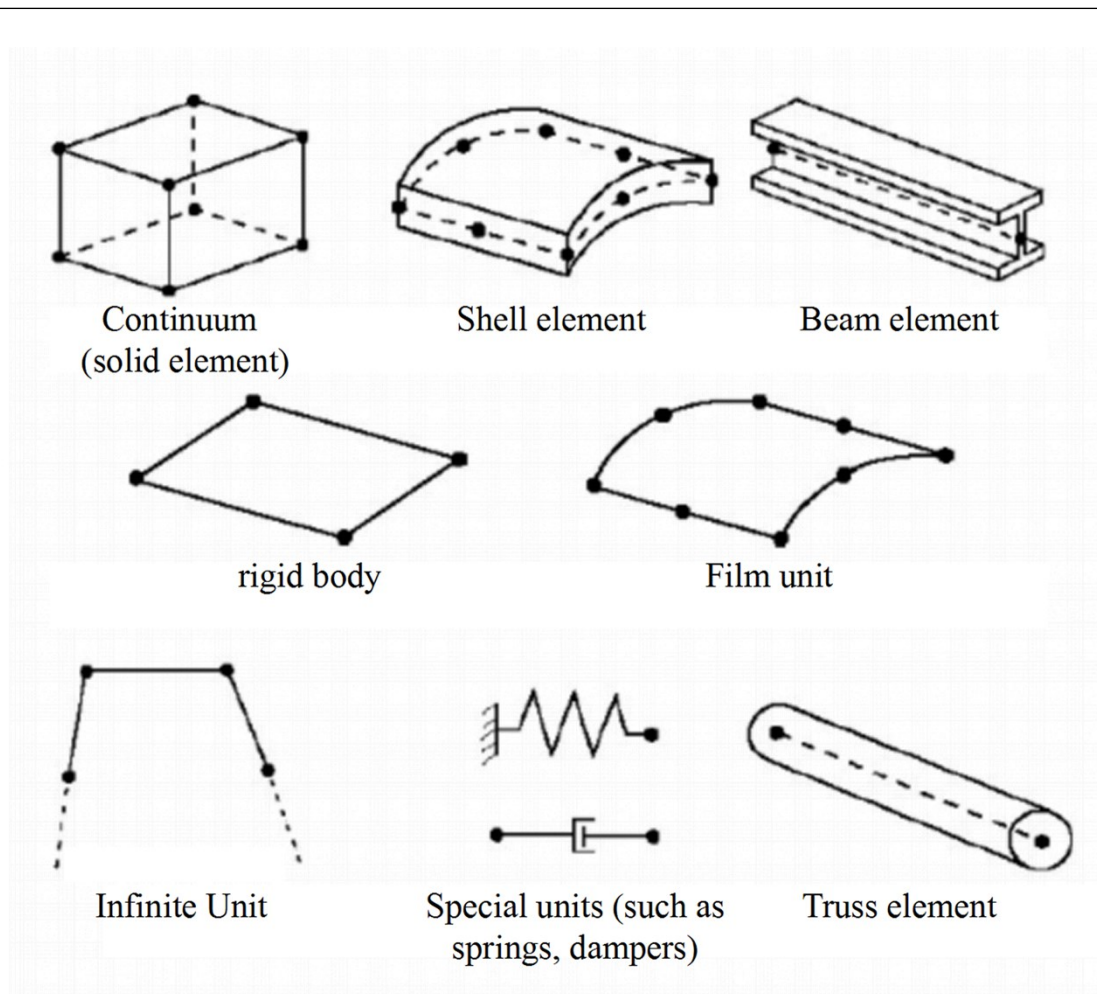


**Fig. S3** The most commonly used elements in ABAQUS.

In ABAQUS/Explicit, the modified quadratic tetrahedral element (C3D10M) is selected, which can be used in contact analysis and elastoplastic analysis. The calculation is highly accurate, but the required calculation cost is also relatively high.

During actual problem analysis, because of the WC anvils, the complexity of the internal structure of the cavity, and the high degree of nonlinearity, the tetrahedral element model has obvious advantages in applicability. The C3D10M element is suitable for explicit secondary analysis and can be compared with the perfect combination of experiments.

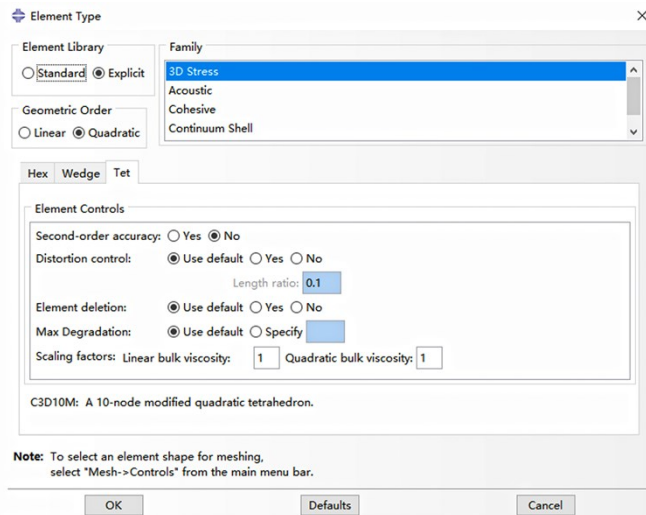


**Fig. S4** Grid type selection operation chart.

#### **4. Selection of unit size**

The accuracy of finite element analysis is largely determined by the choice of element size. Theoretically, after an element type is determined, a grid is densely divided. As more cells are divided, a larger iterative analysis must be carried out, which requires more computing power. This also increases the calculation accuracy and produces a more uniform cloud image distribution, but this exponentially increases the number of calculations and extends the calculation time. Therefore, when simulating and analyzing the diamond synthesis process, we must select different cell sizes to analyze the simulation results. After many experimental comparisons, the assembly block and the WC-anvils were selected as 1.0 mm and 3 mm grid seeds, respectively. For important locations, such as those near the catalyst, the grid area is refined, and high-precision analysis is performed.

---

## 5. Elastic-plastic constitutive relation model

### 5.1 Elastic plasticity of materials

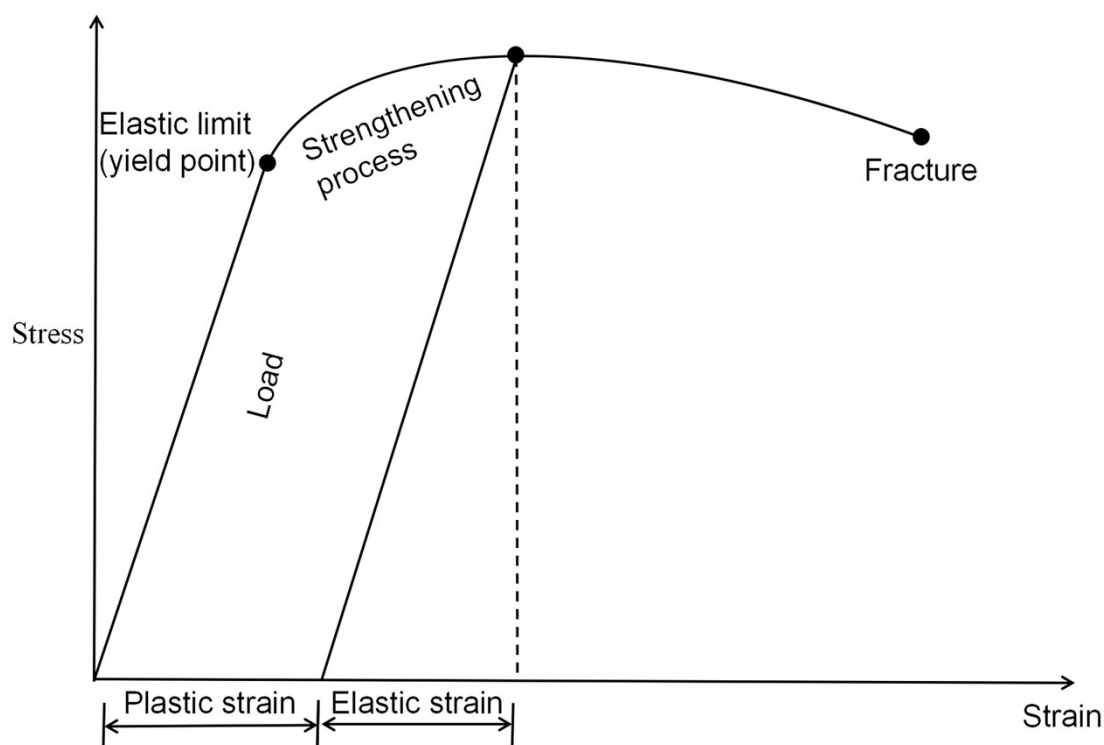


**Fig. S5** Elastic-plastic behavior of materials.

To obtain convincing finite element results, the "constitutive relationship" of a material must be understood. The constitutive relationship generally refers to the universal stress-strain relationship, which includes several aspects such as the yield criterion, hardening criterion, and flow criterion. The ABAQUS program includes hundreds of constitutive (relationship) models. Therefore, it is necessary to select a suitable constitutive model according to the mechanical properties of pyrophyllite and WC-anvil materials. Because of the compression process, the high-pressure cavity structure will undergo greater deformation, and the material will enter a plastic state. To analyze the pressure field in the high-pressure cavity, according to the material's mechanical properties, the correct "constitutive relationship" must be selected. The constitutive model of each component in the high-pressure chamber is shown in Table S1.

**Table S1.** The constitutive model of each component.

Material	Constitutive relationship
Pyrophyllite block	DP plastic model
Steel	Mises Plastic Model
WC-anvils	Rigid body

## 5.2 Mises plasticity model

The Mises yield criterion is a comprehensive concept that considers the first, second, and third principal stresses and can be used to evaluate the fatigue, failure, etc. It is a mechanical concept in elastoplastic mechanics. The yield function of the Mises criterion is expressed as:

$$(\sigma_x - \sigma_y)^2 + (\sigma_y - \sigma_z)^2 + (\sigma_z - \sigma_x)^2 + 6(\tau_{xy}^2 + \tau_{yz}^2 + \tau_{zx}^2) = 2\sigma_s^2 = 6K^2$$

The principal stress is expressed as:

$$(\sigma^1 - \sigma^2)^2 + (\sigma^2 - \sigma^3)^2 + (\sigma^3 - \sigma^1)^2 = 2\sigma_s^2 = 6K^2$$

The yield point of the material is  $\sigma_s$ , and the shear strength of the material is  $K$ .

The equivalent stress is derived as:

$$\bar{\sigma} = \frac{1}{\sqrt{2}} \sqrt{(\sigma_x - \sigma_y)^2 + (\sigma_y - \sigma_x)^2 + (\sigma_z - \sigma_x)^2 + 6(\tau_{xy}^2 + \tau_{yz}^2 + \tau_{zx}^2)} = \sigma_s$$

*Physical meaning*

Mises stress is an equivalent stress for shear deformation, and its value is:

$$\sqrt{\frac{(\alpha_1 - \alpha_2)^2 + (\alpha_2 - \alpha_3)^2 + (\alpha_3 - \alpha_1)^2}{2}}$$

Among them are the first, second, and third principal stresses. This means that when a deformed material reaches a certain strength, the strain of the material transitions from the elastic stage to the yielding stage.

In the principal stress space, the yield surface of Mises criterion is a cylindrical surface with the diagonal of the spatial coordinate axis as the axis, as shown in Fig. S6. The cylinder surface and its interior represent the possible areas of stress. More precisely, when the material inside the cylinder is in the elastic phase, its stress-strain relationship follows the generalized Hooke's law. When the material enters the plastic phase, its stress can only take a value on the cylinder.

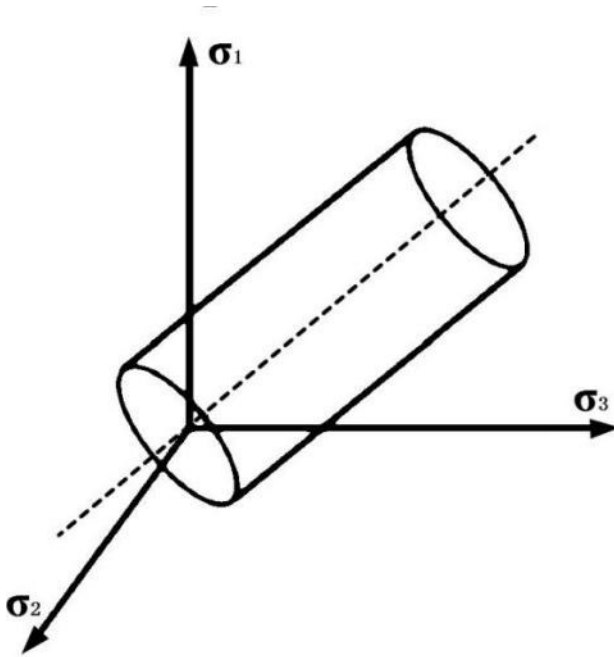


**Fig. S6** Yield surface of the Mises criterion in the principal stress space.

The Mises criterion does not consider the influence of hydrostatic pressure on the yield state and is applicable to soft clays with zero internal friction angles such as metals, alloys, and catalysts. Therefore, the Mises model used in this paper is the constitutive relationship of the pressurized block.

### 5.3 Drucker-Prager (DP) plasticity model

The DP model considers the influence of hydrostatic pressure on the yield of the model, and the yield function is expressed as:

$$f(I_1, \sqrt{J_2}) = \sqrt{J_2} + \alpha I_1 - k = 0$$

Among them  $\alpha$  and  $k$  are the material parameters of the DP model.

In the principal stress space, the DP yield criterion can be regarded as a conical surface whose axis is the diagonal of the space, as shown in Fig. S7.

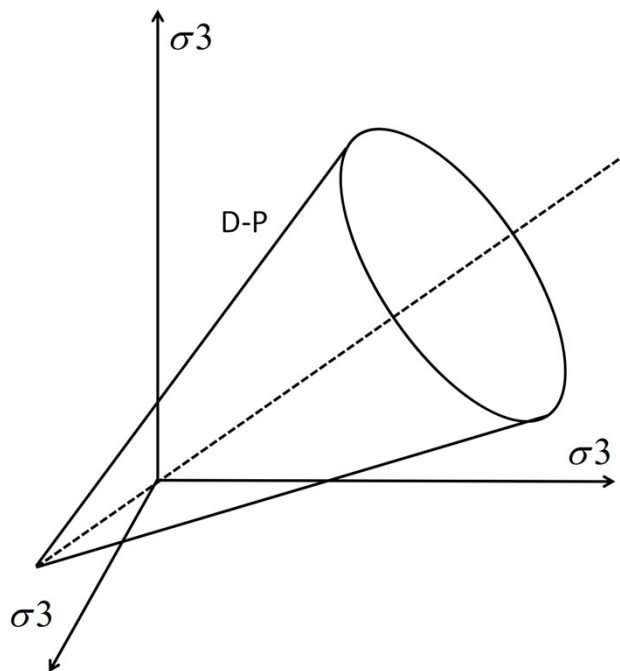


**Fig. S7** Drucker-Prager criterion yield surface in principal stress space.

According to the fitting relationship between the DP yield criterion and the Coulomb-Mohr yield criterion, the material parameters  $\alpha$  and  $k$  can be expressed by the viscous force  $C$  and the internal friction angle  $\phi$ :

$$\alpha = \frac{2\sin\phi}{\sqrt{3}(3 - \sin\phi)} \quad k = \frac{6C \cos\phi}{\sqrt{3}(3 - \sin\phi)}$$

The DP model is especially suitable for classical models of geotechnical materials using two model parameters: cohesion and internal friction angle; therefore, this paper used the DP model to define the constitutive relationship of pyrophyllite.

## 6. Finite element model

Diamonds were synthesized in an SPD-6 $\times$ 1200 cubic anvil high-pressure apparatus (CHPA) by a temperature gradient growth (TGG) method under HPHT conditions. The experimental equipment, and the synthetic block placement diagram are shown in Fig. S8.

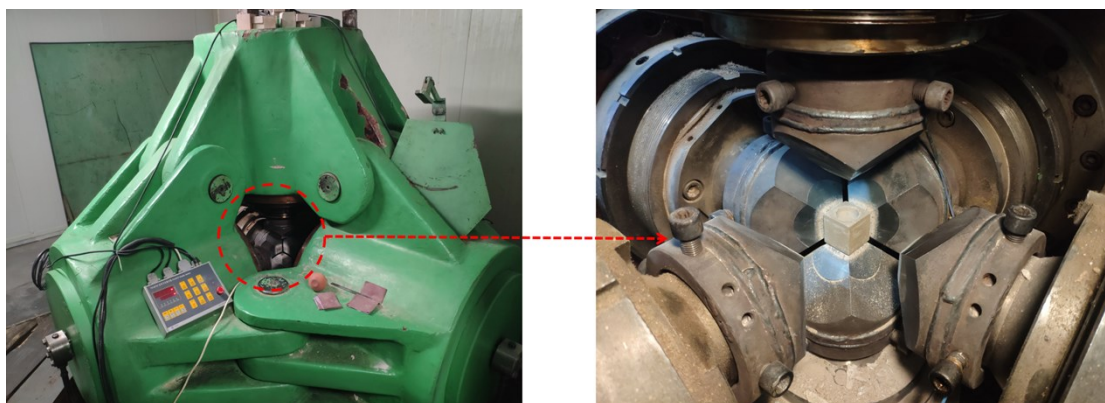


**Fig. S8** SPD-6×1200 Cubic anvil high-pressure apparatus and synthesis block placement diagram.

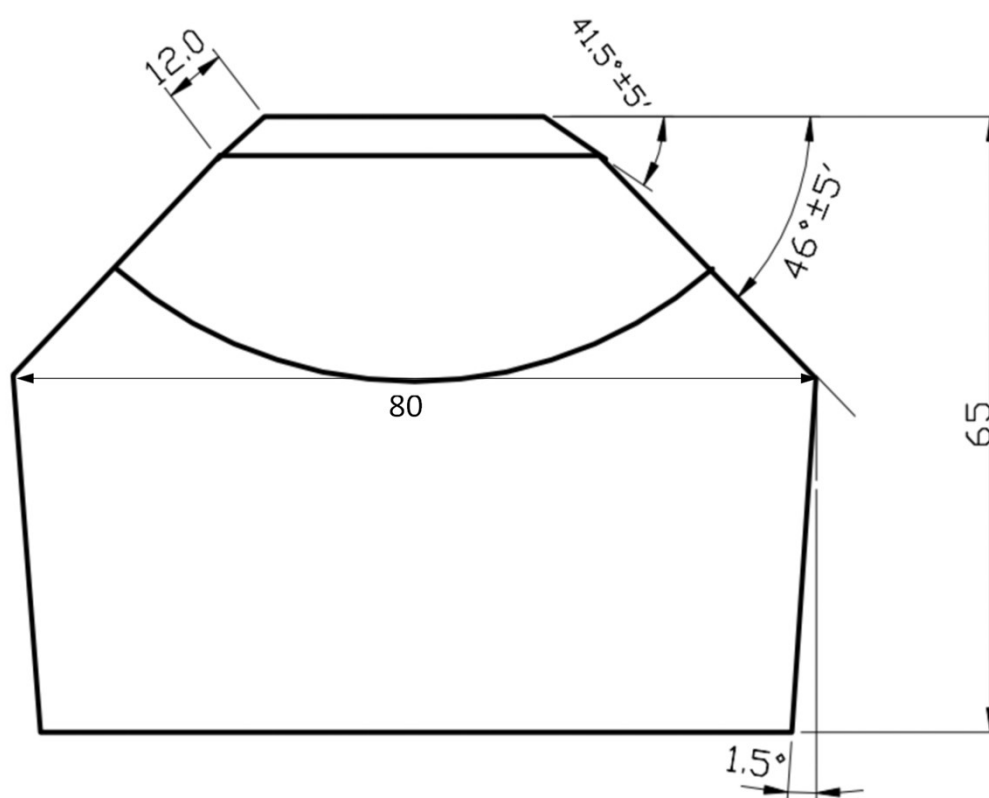


**Fig. S9** Engineering drawing of the anvil design.

The size of the solid pyrophyllite block used in the experiment of the analysis object is 38 mm×38 mm×38 mm, and its geometric model was established by Solidworks 3D drawing software. Fig. S10 (a) shows the finite element model of the tungsten carbide WC-anvils, and Fig. S10 (b) shows the finite element model of the pressurized block cavity.

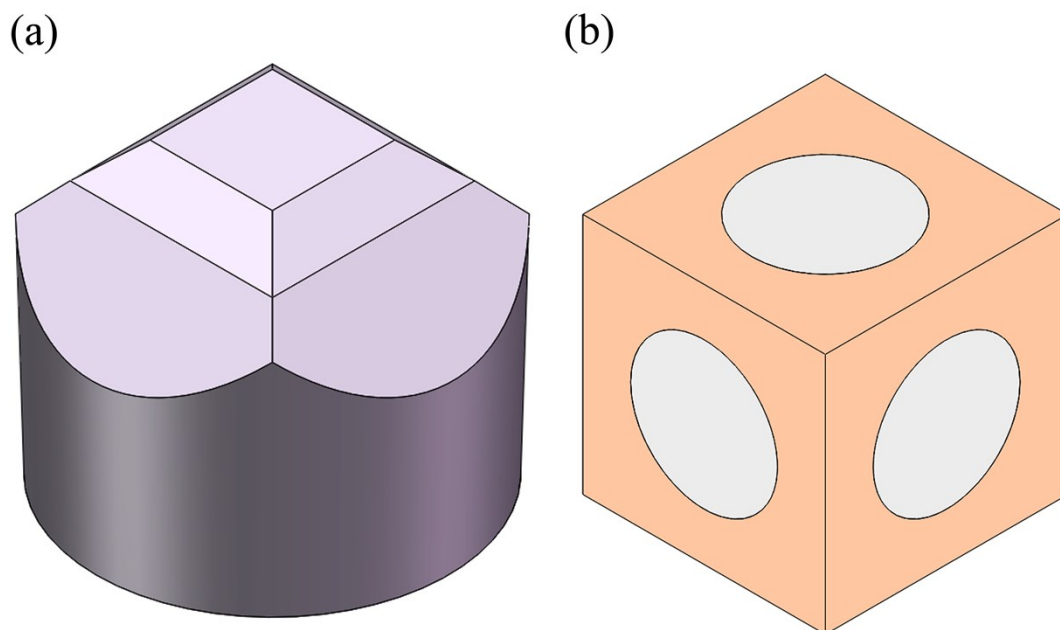


**Fig.S10** (a) Finite element model of the WC-anvil. (b) Finite element model of a pyrophyllite solid block.

The assembly process of the finite element model of the SPD-6×1200 cubic anvil high pressure apparatus: After the finite element model of the tungsten carbide WC-anvils and the pyrophyllite solid block were built according to the actual working conditions, they were assembled. The assembly relationship between the tungsten carbide WC-anvils and the solid block is that the WC-anvil surface overlaps with the six surfaces of the solid block. The direction of the center axis of the WC-anvils is the same as the direction of the central axis of the assembly block, and it is symmetrical. Fig. S11 shows the finite element model of the SPD-6×1200 cubic anvil high-pressure apparatus.

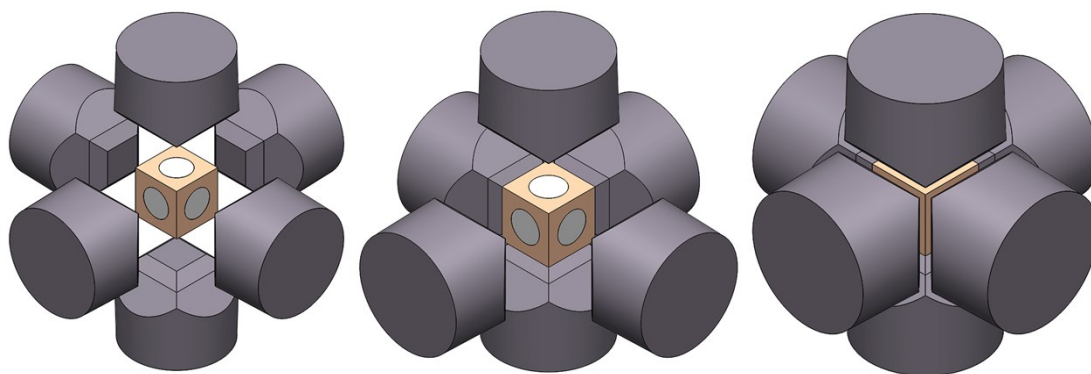


**Fig. S11** Finite element model of CPHA.

To decrease calculation time and costs, we simplified the model according to its geometric symmetry to a 1/8 finite element model and imported it into the ABAQUS finite element simulation software for meshing and other operations. Fig. S12 (a) is a 1/2 finite element model, Fig. S12 (b) is a 1/4 finite element model, Fig. S12 (c) is a 1/8 finite element model, Fig. S12 (d) is a SPD-6×1200 cubic anvil high-pressure apparatus meshing diagram, and Fig. S12 (e) is the meshing diagram of a pyrophyllite solid block.

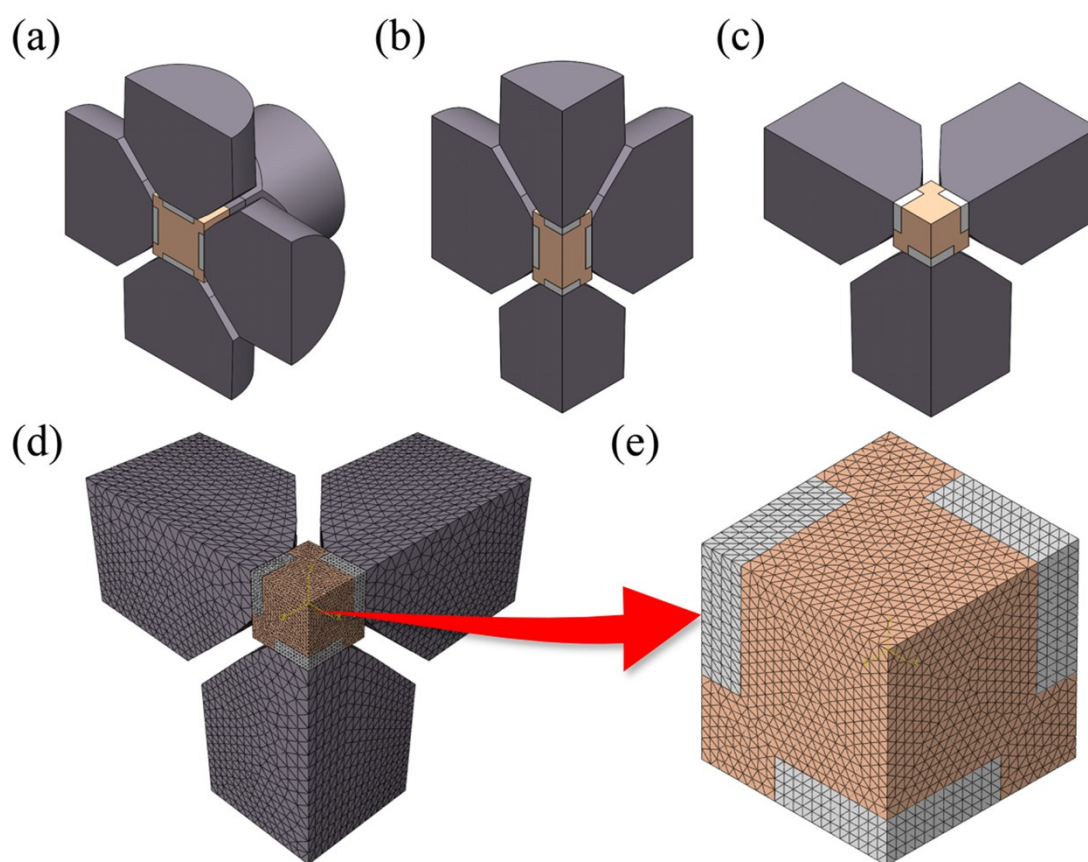


**Fig.S12** (a) 1/2 finite element model. (b) 1/4 Finite element model. (c) 1/8 Finite element model. (d) Grid division diagram of CPHA. (e) Grid division diagram of an assembly cell.

## 7. Principle of mass support

The high-pressure equipment was designed using the principle of large mass support. As shown in Figure S11, the bottom area  $S_1$  is much larger than  $S_2$ , and the

corresponding relationship between pressure and area is:  $P_1 S_1 = P_2 S_2$ . The pressure applied to the bottom surface of the anvil is  $P_1$ , and since  $S_1$  is much greater than  $S_2$ , a pressure much greater than  $P_1$  can be obtained on the top surface of the anvil. The higher the ratio of  $S_1$  to  $S_2$ , the higher the corresponding pressure; therefore, the design principle of CPHA is to use the principle of large mass support to obtain a super high pressure through the huge difference between the top surface area of the cylinder and the anvil.

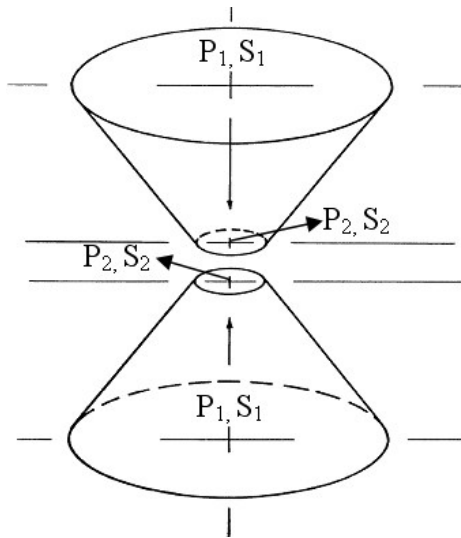


**Fig. S13** Schematic diagram illustrating the principle of mass support

According to the principle of mass support, when the oil pressure was 70 MPa, the bottom surface pressure of the WC-anvils was calculated according to the proportional relationship of  $P_1 S_1 = P_2 S_2$  to be 1.4 GPa (where  $P_1$  is the oil pressure,  $S_1$  is the cylinder area,  $P_2$  is the load applied on the bottom surface of the WC-anvils, and  $S_2$  is the area of the bottom surface of the WC-anvils).

## 8. Boundary conditions

The simulation used finite element display dynamics analysis. When the applied load was 70 MPa, the bottom surface pressure of the WC-anvils was calculated by the principle of mass support to be 1.4 GPa, which was evenly distributed over the bottom of the WC-anvils. Fig. S14 shows the load analysis diagram of the six-sided WC-anvils.

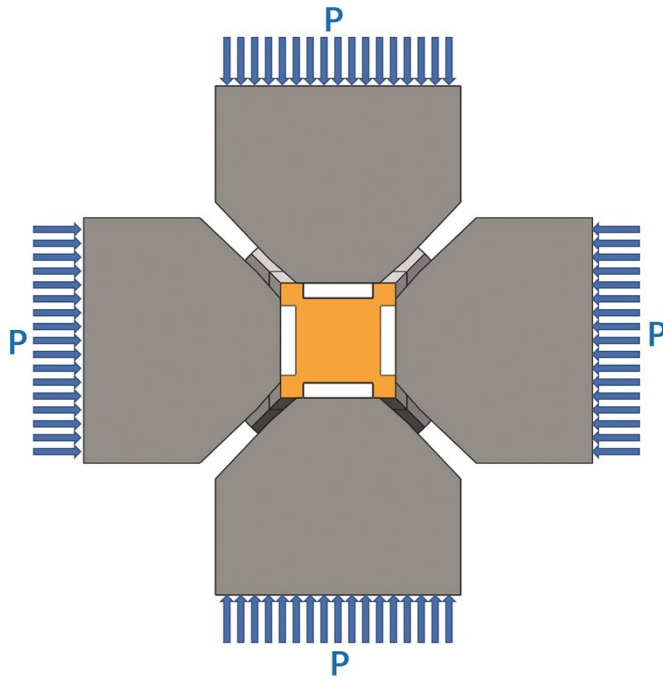


**Fig. S14** Load analysis diagram of the WC-anvil.

When establishing a finite element model, to decrease calculation time and costs, we simplified the model to a 1/8-scale model. When defining the boundary conditions, we defined the symmetric boundary conditions. XSYMM is the symmetry about the plane perpendicular to the x-axis ( $U_1=UR_2=UR_3=0$ ), ZSYMM is the symmetry about the plane perpendicular to the z-axis ( $U_3=UR_1=UR_2=0$ ), and YSYMM is the symmetry about the plane perpendicular to the y-axis ( $U_2=UR_1=UR_3=0$ ).

To define the interactions, select the general contact type, and to set the mechanical contact properties, the friction coefficient used the penalty function, and the value was set to 0.75.

## 9. Material parameters

The selection of material parameters directly affects the accuracy of the simulation results. The determination of the mechanical parameters of materials under high temperature and high pressure is the focus of this work. The representative composition of pyrophyllite is listed in Table S2. The elastoplastic properties of pyrophyllite used in this article were obtained by Dr. Rui Li through uniaxial compression, triaxial compression, and shear experiments at the Wuhan Institute of Rock and Soil

Mechanics, Chinese Academy of Sciences.[1] The calculated elastic modulus, Poisson's ratio, cohesion, and internal friction angle of pyrophyllite at different firing temperatures are shown in Table S3.

**Table S2.** Representative composition of pyrophyllite/%

SiO <sub>2</sub>	TiO <sub>2</sub>	Al <sub>2</sub> O <sub>3</sub>	Fe <sub>2</sub> O <sub>3</sub>	FeO	HgO+
49.09	1.35	41.39	0.08	0.31	6.8

**Table S3.** Material parameters of pyrophyllite block

Roasting temperature/°C	Elastic modulus/GPa	Average Poisson's ratio	Cohesion /MPa	Internal friction angle/(° )
25	2.56	0.12	6.75	31.84
200	2.64	0.12	11.90	24.8
240	2.87	0.12	13.87	20.68
700	5.42	0.12	18.95	27.10

According to the experimental values, the material parameters corresponding to a baking temperature of 240°C were selected.

When setting the elastoplastic model parameters, the DP model in ABAQUS requires 3 input parameters: internal friction angle, expansion angle, and yield stress. When the DP model is used for calculations, the cohesion (c) is the most important material parameter because it directly affects the calculation results of the model.

In this article, we did not study the stress distribution in the WC-anvils, using an elastic modulus of 720 GPa, and Poisson's ratio of 0.3.

---

## 10. Experiment data

**Table S4.** The effect of  $h$  on cavity pressure when  $S$  is fixed.

Diameter: $d$ (mm)	Height: $h$ (mm)	Cavity pressure (GPa)
23	0	5.700
23	1	5.885
23	2	6.142
23	3	6.531
23	4	7.145
23	5	7.790

**Table S5.** When  $h$  is fixed at 1 mm, the effect of  $d$  on cavity pressure

Diameter: $d$ (mm)	Height: $h$ (mm)	Cavity pressure (GPa)
15	1	5.783
17	1	5.792
19	1	5.823
21	1	5.859
23	1	5.885

**Table S6.** When  $h$  is fixed at 2 mm, the effect of  $d$  on cavity pressure.

Diameter: $d$ (mm)	Height: $h$ (mm)	Cavity pressure (GPa)
15	2	5.815
17	2	5.855
19	2	5.929
21	2	6.013
23	2	6.14

**Table S7.** When  $a$  is fixed, the effect of shape (square) on cavity pressure.

Side length: $a$ (mm)	Height: $h$ (mm)	Cavity pressure (GPa)
20.38	1	5.885

---

20.38	2	6.168
20.38	3	6.550
20.38	4	7.091
20.38	5	7.709

---

### **Notes and references**

[1]. R. Li, H. A. Ma, Q. G. Han, et al. Simulation of pressure distribution in a pyrophyllite high-pressure cell by finite-element analysis. *High Pressure Research.*, 2007, 27(2), 249-257.